






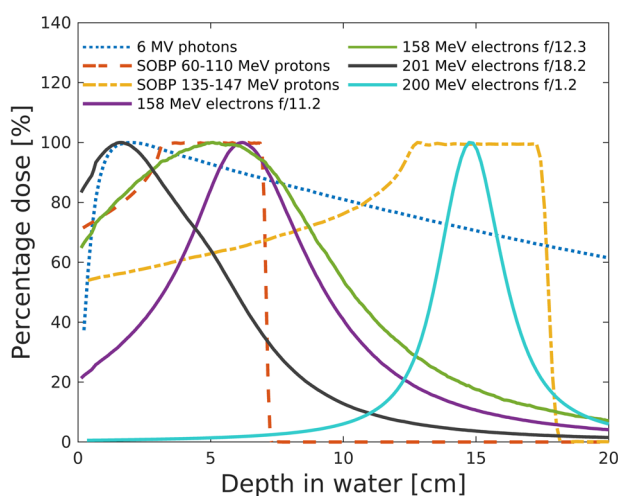
## An experimental study of focused very high energy electron beams for radiotherapy

Karolina Kokurewicz<sup>1</sup>, Enrico Brunetti<sup>1</sup>, Alessandro Curcio<sup>2</sup>, Davide Gamba<sup>2</sup>, Luca Garolfi<sup>2</sup>, Antonio Gilardi<sup>2,3,4</sup>, Eugenio Senes<sup>2,5</sup>, Kyrre Ness Sjobak<sup>2,6</sup>, Wilfrid Farabolini<sup>2,7</sup>, Roberto Corsini<sup>2</sup> & Dino Anthony Jaroszynski<sup>1</sup>

Very high energy electron (VHEE) beams have been proposed as an alternative radiotherapy modality to megavoltage photons; they penetrate deeply without significant scattering in inhomogeneous tissue because of their high relativistic inertia. However, the depth dose distribution of a single, collimated VHEE beam is quasi-uniform, which can lead to healthy tissue being overexposed. This can be largely overcome by focusing the VHEE beam to a small spot. Here, we present experiments to demonstrate focusing as a means of concentrating dose into small volumetric elements inside a target. We find good agreement between measured dose distributions and Monte Carlo simulations. Focused radiation beams could be used to precisely target tumours or hypoxic regions of a tumour, which would enhance the efficacy of radiotherapy. The development of new accelerator technologies may provide future compact systems for delivering these focused beams to tumours, a concept that can also be extended to X-rays and hadrons.

<sup>1</sup>SUPA, Department of Physics, University of Strathclyde, G4 0NG Glasgow, UK. <sup>2</sup>CERN, European Organization for Nuclear Research, 1211 Geneva 23, Switzerland. <sup>3</sup>University of Napoli Federico II, Via Claudio 21, 80125 Napoli, Italy. <sup>4</sup>National Institute for Nuclear Physics (INFN), Section of Napoli, Napoli, Italy. <sup>5</sup>John Adams Institute and University of Oxford, The Denys Wilkinson Building, Keble Road, Oxford OX1 3RH, UK. <sup>6</sup>University of Oslo, 0316 Oslo, Norway. <sup>7</sup>Saclay Nuclear Research Centre, Gif-Sur-Yvette Cedex, 91190 Saclay, France. ✉email: [enrico.brunetti@strath.ac.uk](mailto:enrico.brunetti@strath.ac.uk); [d.a.jaroszynski@strath.ac.uk](mailto:d.a.jaroszynski@strath.ac.uk)

The main objective of radiotherapy is to kill cancer cells while sparing normal tissue from damage<sup>1</sup> and minimising the creation of secondary cancers. This is usually achieved through modalities such as volumetric modulated arc therapy (VMAT)<sup>2</sup>, stereotactic radiosurgery (SRS)<sup>3</sup>, intra-operative radiation therapy (IORT)<sup>4,5</sup> or brachytherapy.<sup>6</sup> To reduce irradiation of healthy tissue and ensure complete irradiation of tumours<sup>7</sup>, dose must be delivered precisely in such a way that it conforms to the tumour shape. A common approach is to physically shield healthy tissue and apply multiple beams to irradiate tumours from different directions<sup>8</sup>. Megavoltage (MV) X-rays (4–25 MV) are the commonly used radiation for treating cancers. As illustrated in Fig. 1, the depth–dose distribution produced by a single X-ray beam is high at the entrance and reduces exponentially with depth. Proton and ion beams can improve the contrast between the doses in the tumour with that in healthy tissue, especially in the distal region, by taking advantage of the Bragg peak<sup>9,10</sup>. Better conformity is achieved using a spread out Bragg



**Fig. 1 Simulations of axial dose distributions in a water phantom for different beam geometries and energies.** (i) Collimated 6 MV photons, (ii) 60–110 MeV and (iii) 135–147 MeV protons (SOBP), 158 MeV electron beams focused in the horizontal plane with (iv)  $f/11.2$  and (v)  $f/12.3$  (vi) 201 MeV focused in the horizontal plane with  $f/18.2$  and (vii) 200 MeV symmetrically focused with  $f/1.2$ . The  $f$ -number is a measure of focusing strength defined as  $f/D$ , where  $D$  is the beam diameter at the focusing optics and  $f$  is the focal length of the lens, as in optics. The dose is normalised to the peak dose of each individual depth–dose profile.

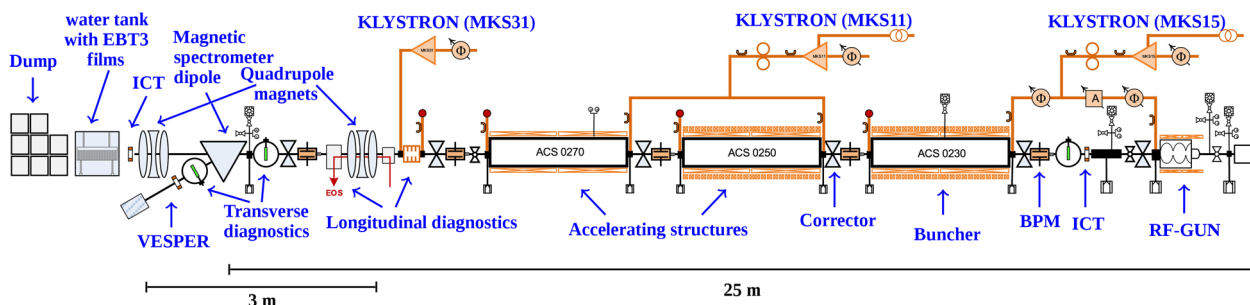
peak (SOBP) that is produced by varying the beam energy (e.g. from 60 to 110 MeV and 135 to 147 MeV). However, this results in a build-up of an anterior dose<sup>11</sup>, as shown in Fig. 1. Moreover, the dose distribution is sensitive to tissue density inhomogeneity, which results in range uncertainties<sup>12</sup> and potentially under-irradiation of the tumour, or over-irradiation of healthy tissue<sup>13</sup>.

Over the last 20 years, very high-energy electrons (VHEEs), in the range of 60–250 MeV<sup>14</sup>, have been considered as a promising alternative to photons for the treatment of deep-seated tumours<sup>15–19</sup>. Low-energy electrons (<MeV), from current clinical linacs<sup>20</sup>, have shallow penetration depths and thus are only suitable for treatment of superficial tumours<sup>21</sup> or for intra-operative radiotherapy<sup>22</sup>. VHEEs, in contrast, are very penetrating due to their high inertia, which enables them to reach deep-seated tumours<sup>19,23–27</sup>. Their dose is characterised by a sharp transverse penumbra and low scattering at tissue interfaces<sup>14,23,28</sup>, compared with current low-energy clinical electrons<sup>29,30</sup>. VHEE beams are also relatively easy to form into pencil beams or scan using electromagnet deflectors<sup>15</sup>. However, VHEE accelerators are currently relatively large and expensive, compared with 4–22 MeV clinical accelerators, but compact VHEE sources should become available with the development of new technologies such as X-band radio-frequency (RF) accelerators<sup>31</sup> and laser-plasma wakefield accelerators<sup>32–36</sup>.

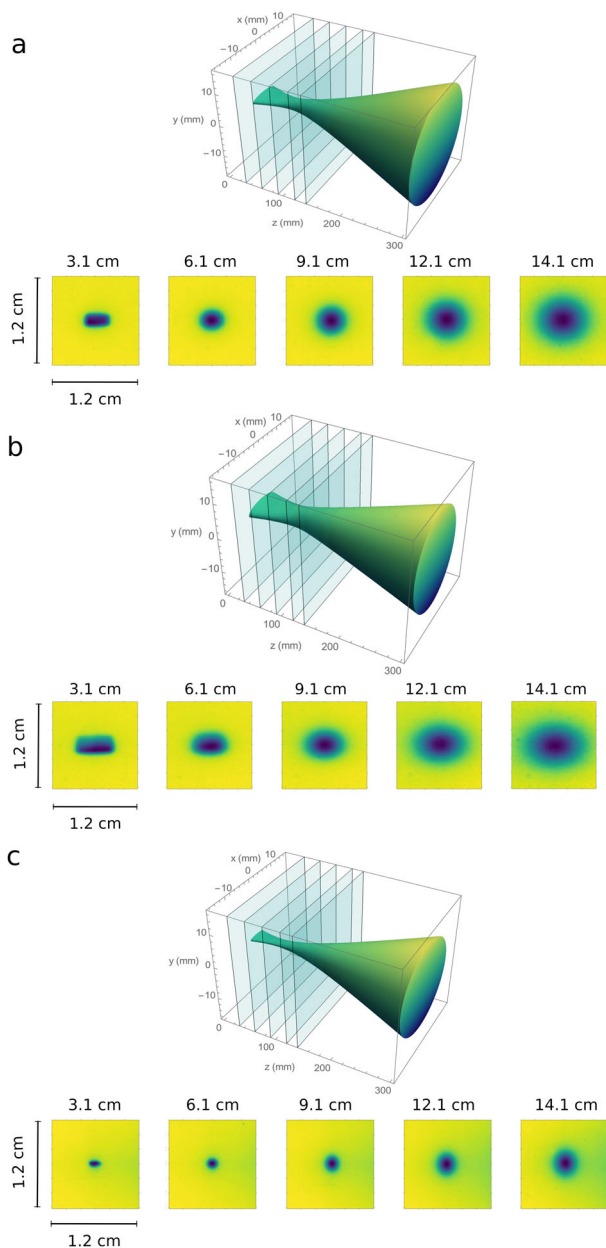
The depth–dose distribution of collimated VHEE beams is nearly uniform<sup>19,26</sup> and several methods have been investigated to improve it. Theoretical and experimental studies have shown that lateral scattering of low-energy (<70 MeV) electron beams can be reduced by imposing a longitudinal or transverse magnetic field on the medium<sup>37–39</sup>, which results in a depth–dose profile that resembles a degraded Bragg peak. Recent Monte Carlo (MC) studies have shown that for VHEEs this dose enhancement at depth can be obtained simply by externally focusing the electron beam using a magnetic lens<sup>19</sup>. As in optics, we define the  $f$ -number as  $f/D$ , where  $D$  is the beam diameter on the focusing optics and  $f$  is the focal length of the lens. Here we present experimental measurements of the depth–dose distribution of VHEE beams focused in a water phantom for several  $f$ -numbers and electron energies, and compare these results with theoretical predictions.

## Results and discussion

The experiment has been performed at the CERN Linear Electron Accelerator for Research (CLEAR) beamline<sup>40</sup>, which is based on an S-band RF accelerator that delivers quasi-mono-energetic electron beams with energies between 60 and 220 MeV. The experimental layout is shown in Fig. 2 and more details given in



**Fig. 2 The CLEAR accelerator, beamline and schematic of the experimental setup.** The electron beam (travelling from right to left) is produced by a radio-frequency (RF) gun and accelerated up to 220 MeV by three 4.5 m long S-band accelerating structures driven by 2 modulators/klystrons (MKS11 and MKS15). A third klystron (MKS31) can power a transverse deflector. The first structure (Buncher) can also be used to longitudinally compress the electron bunches. Beam diagnostics include a beam position monitor (BPM) and integrating current transformer (ICTs) to measure the charge at different stages. The electron beam energy is measured using a dipole electromagnet that also directs the beam to the VESPER test bench. Two triplets of quadrupole magnets focus the beam inside the water phantom, which is placed at the end of the beamline and is shown in detail in Fig. 5.



**Fig. 3** 3D reconstruction of the dose profiles based on measured radiation beam profiles using EBT3 films. **a** 158 MeV with  $f/11.2$ , **b** 158 MeV with  $f/12.3$  and **c** 201 MeV with  $f/18.2$  focused beams with selected EBT3 film samples placed at depths of 3.1, 6.1, 9.1, 12.1, 14.1 cm in water.

Methods. The electron beam is first expanded by making it diverge over a distance of about 3 m using three quadrupole magnets placed after the last RF deflecting cavity (Fig. 2). The beam is then focused by a second quadrupole triplet into a water phantom, which is placed 21.5 cm downstream of the last quadrupole magnet. The magnetic field strength and aperture size of the quadrupoles only allows focusing with a short focal length in one plane, which is chosen to be horizontal. The beam is collimated or diverges slightly in the vertical plane, resulting in a line focus. Symmetric focusing could have been achieved by upgrading the power supplies of the first quadrupole triplet and employing larger aperture quadrupoles in the second triplet. However, this was not possible in the allocated experimental

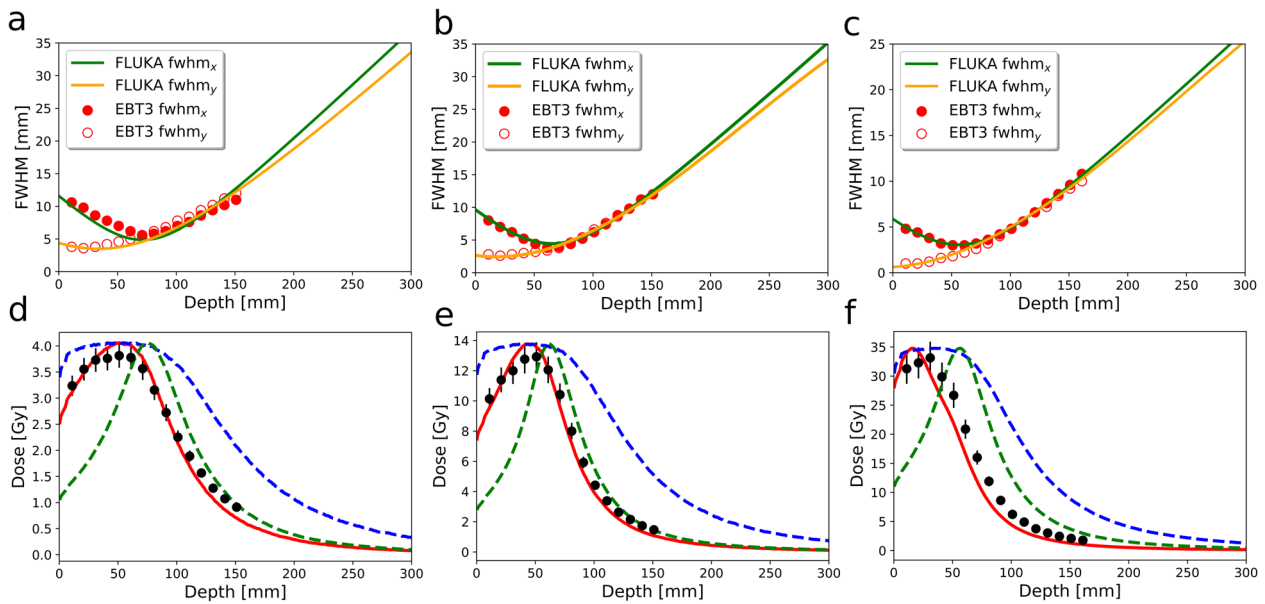
time. After the final quadrupole magnet, the beam passes through a 0.1 mm thick aluminium window into ambient air, and then through an integrating current transformer (ICT - Bergoz, ICT-055-070-5.0, SN 3350), and finally into the phantom. The ICT records the total charge of the beam entering the phantom. The transverse dose profile is measured at different depths in the phantom using a stack of 16 Gafchromic® films (EBT3, Ashland ISP Advanced Materials) spaced by 1 cm, as discussed in Methods.

**Measured dose profiles.** Figure 3 shows beam for selected irradiated films spaced by 3 cm (every third film apart from the last film, which is spaced by 2 cm). A 3D simulated reconstruction of the dose distribution is also included, which is based on fits of the sizes measured in the horizontal and vertical planes across the whole film stack. The quadrupole magnetic fields are set to produce a focus at a distance of 14 cm for 158 MeV, and  $f/11.2$  and 10 cm for 158 MeV focused with  $f/12.3$  and 201 MeV focused with  $f/18.2$ , from the phantom entrance in air, as measured using an optical transition radiation (OTR) screen.

The beam size at the final quadrupole has been varied to obtain different focusing strengths. Here we present results for  $f/11.2$  and  $f/12.3$  (158 MeV), and  $f/18.2$  (201 MeV). Since the CLEAR beamline is not designed for short focal lengths (because of the small diameter of the vacuum pipe), the beam is clipped by the walls of the metal pipe and rectangular drift-chamber in the magnetic spectrometer, resulting in a rectangular beam profile in the vertical plane on the EBT films. In the horizontal plane, the beam profile is approximately Gaussian for  $f/12.3$  and  $f/18.2$ , but rectangular for  $f/11.2$ . The full-width at half-maximum (FWHM) and depth-dose profiles obtained from the films and FLUKA MC simulations are shown in Fig. 4. The simulated curves are obtained using the beam size measured at the phantom entrance, the focus position in air and the total charge recorded on the ICT monitor, as discussed in Methods. Measurements and simulations show that the maximum of the dose distribution is located about 5–6 cm inside the phantom at a depth corresponding to the position of the beam focus. The smallest spot size measured in the plane where the beam is focused is 3 mm FWHM for 201 MeV energy (Table 1).

Our previous theoretical study showed that for symmetrically focused beams the spot size at the focus decreases with  $f$ -number<sup>19</sup> along the beam direction and increases in the transverse direction, resulting in an asymmetric shape of the high-dose volumetric element. However, for a line focus, as shown in this study, this effect is obscured. As the beam propagates further into the phantom the transverse shape becomes symmetric due to scattering, which also shifts the focus towards the phantom entrance, with respect to its position in air, by 7.6, 2.3 and 4.0 cm, for  $f/11.2$ ,  $f/12.3$  and  $f/18.2$ , respectively.

Simulations have also been performed for a collimated beam, indicated by the blue curves in Fig. 4, with the beam size corresponding to the FWHM in the plane where the beam is focused. Focusing enhances the peak dose, compared with collimated beams, by 6, 4.2 and 8.2 times for  $f/11.2$ ,  $f/12.3$  (158 MeV) and  $f/18.2$  (201 MeV), respectively (Table 1). For higher energies, symmetric focus shifts the maximum further into the phantom, while the peak dose decreases due to scattering and therefore becomes lower than for a beam focused in one plane for the same incident beam charge. However, for symmetrically focused beams (the green curves in Fig. 4), the peak dose is more pronounced than for the experimental curves and provides a more favourable dose distribution by reducing the proximal and distal dose.



**Fig. 4 Measured dose distributions.** Beam envelope (a–c) and depth dose in the water phantom (d–f) for experimental focused beams. (a, d) 158 MeV focused with  $f/11.2$ , (b, e) 158 MeV focused with  $f/12.3$ , and (c, f) 201 MeV focused with  $f/18.2$ . Solid red curves are simulated depth-dose profiles for beams focused only in the horizontal plane. Dashed green lines are simulated dose profiles obtained for symmetric focusing, while the dashed blue lines represent collimated beams. The depth-dose curves for collimated and symmetrically focused beams are normalised to the peak dose of the line focus. The vertical lines in depth-dose profile for experimental beam indicate measurement uncertainties.

**Table 1 Peak dose and full-width at half-maximum (FWHM) obtained from x and y projections of the transverse beam profile at the focus depth, for different beam geometries obtained with the FLUKA MC code.**

	Peak dose (Gy) and FWHM (mm)		
	158 MeV, $f/11.2$	158 MeV, $f/12.3$	201 MeV, $f/18.2$
Line focus	13.82 Gy	4.07 Gy	34.65 Gy
Symmetric focus	10.03 Gy	3.03 Gy	11.98 Gy
Collimated beam	2.32 Gy	0.92 Gy	4.21 Gy
FWHM <sub>x</sub>	3.0 mm	5.6 mm	3.8 mm
FWHM <sub>y</sub>	2.0 mm	5.9 mm	3.7 mm

## Conclusion

We measured the depth-dose profile of 158 and 201 MeV electron beams focused into a water phantom, demonstrating on-axis dose enhancement at a depth of 5–6 cm, which validates theoretical predictions that focused VHEE beams concentrate dose into a well-defined volume deep in tissue. The dose delivered to surrounding tissue is distributed over a larger volume, which reduces surface and exit doses compared with collimated beams. At fixed electron energy, the increase of the peak dose is more pronounced for smaller  $f$ -numbers ( $f/11.2$  for the results presented here). Symmetrically focused beams would require higher charge, but the peak dose can be delivered deeper into the body. VHEE beams are a promising modality in radiotherapy of deep-seated tumours where other modalities may not be appropriate due to strong scattering at tissue interfaces, high skin dose or weak penetration.

The focusing method can also be used to deliver therapeutic doses at high rates (FLASH<sup>41</sup> radiotherapy), a regime accessible with the accelerator at the CLEAR user facility. Treatment can be

administered using a single beam, potentially reducing the detrimental effects of irradiating healthy tissue, and therefore lowering the risk of radiation-induced secondary cancers, compared with conventional treatment methods combined with FLASH therapy. Deposition of high dose into a small volume by a single beam can also increase precision. Furthermore, similar geometric effects can be observed with other modalities, such as photons and protons, as shown in Supplementary Fig. 1a, b and c, d, respectively. It has been shown previously that a focused photon beam can be produced simply by passing a focused VHEE beam through a bremsstrahlung converter<sup>42</sup>. The resulting dose distribution of the focused gamma rays is similar to that of a focused VHEE beam<sup>42</sup>.

Millimetre long laser-plasma wakefield accelerators<sup>43</sup> are currently capable of producing quasi-mono-energetic electron beams<sup>44</sup> with a few tens of picocoulomb bunch charge<sup>45</sup>, femtoseconds bunch durations<sup>46–48</sup> and in the 100 MeV to GeV energy range<sup>49</sup>. They have been already used for dosimetry studies using VHEE fields, which show excellent agreement with EBT3 film responses using clinical accelerators<sup>26</sup>. Most medical accelerators are based on 3 GHz, S-band cavities with accelerating gradients less than 100 M/V. However, X-band linacs, operating at 12 GHz, can have higher accelerating gradients, and are potentially more compact. The experiments presented here have been carried out in a laboratory environment, which differs from a clinical setting. However, production of secondary radiation is largely absent because beam-shaping components, as used in conventional clinical accelerators, are not required. Focusing of the electron beam only requires quadrupole magnets, which do not intercept the beam.

## Methods

**Accelerator and beam focusing system.** The experiment has been conducted at the CERN CLEAR beamline. An electron beam with an energy up to 220 MeV is passed through two sets of triplet electromagnetic quadrupoles (EMQs), with specifications given in Table 2, and focused inside a phantom ( $30 \times 30 \times 30 \text{ cm}^3$

PMMA tank filled with water) mounted on a movable stage to allow precise translation in the direction perpendicular to the beam propagation axis (Fig. 5).

When the phantom is moved out, the electron beam passes through an OTR screen<sup>50</sup> mounted on a stage that can also be translated along the beamline axis. This is imaged onto a CCD camera, which enables measurement of the beam envelope in air. The phantom is placed at the end of the beamline and the electron beam profile is measured at different depths using a stack of 16 EBT3 films immersed in water and spaced by 1 cm. These are cut into 21.5 × 6.75 cm<sup>2</sup> strips, which enables several shots to be recorded on the same strip simply by moving the phantom transversally. The water phantom entrance is placed 32.8 cm from the centre of the last quadrupole. The electron beam passes through a 0.1 mm thick aluminium window and propagates in air for 21.5 cm, passing through a charge monitor unit prior to the phantom, as shown in Fig. 5a. Measurements were carried out for 158 and 201 MeV electron energies. In each case, the electron beam Twiss parameters<sup>51,52</sup> (Table 3) were measured using the quadrupole scan technique<sup>53</sup> and the beam transport is optimised using the software package MAD-X<sup>54</sup>. Reconstructions of the beam envelopes based on beam Twiss parameters and optics for all beam geometries are shown in Supplementary Fig. 2.

As the CLEAR beamline is not designed for short focal lengths, it was decided to focus the beam only in one plane, which produces a line focus at a chosen reference depth (in vacuum) and inside the water phantom. The EMQ settings for all *f*-numbers are shown in Table 4. The focal length used to calculate the *f*-number is defined as the distance from the centre of the final quadrupole to the focal spot position.

**Dosimetry.** EBT3 films are irradiated with a charge of 0.92 nC (8 shots) for *f*/11.2, 0.58 nC (10 shots) for *f*/12.3 and 0.62 nC (10 shots) for *f*/18.2, measured with the uncertainty of 2%. After exposure, the films are read using an Epson Expression 10000XL flatbed scanner. The digitised images are processed using a 2D Wiener filter to remove scanner noise. The background is defined as the average pixel value of four regions with dimensions of 5 × 5 pixels at the corners of each spot. The dose is calculated as the peak value using the red colour channel, which provides the most sensitive response up to 8 Gy, using the formula

$$D = a \cdot \text{netOD} + b \cdot \text{netOD}^n, \quad (1)$$

where netOD is the change in optical density before and after irradiation, given by  $\text{netOD} = \log_{10}(\text{PV}_{\text{before}}/\text{PV}_{\text{after}})$ , where PV is a pixel value. The other coefficients are  $a = 9.1$ ,  $b = 58$  and  $n = 3.2$ , obtained by calibrating films from the same batch (lot 06141702) at the Physikalisch-Technische Bundesanstalt (PTB) research accelerator that produces electrons with energies up to 50 MeV<sup>55</sup>.

**Monte Carlo simulations.** MC simulations with the code FLUKA<sup>56</sup> have been performed to model the depth dose distribution in water for the same configurations as used in the experiments. The beam size at the front of the water tank is

**Table 2 Quadrupole magnet specification.**

Nominal gradient (T/m)	11.2
Inscribed radius (mm)	29
Integrated gradient (T/m)	2.53
Nominal current at 11.2 T/m (A)	200

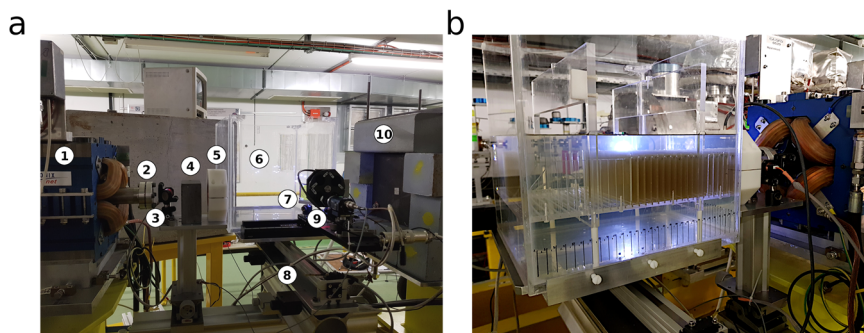
taken as the FWHM of the dose profile measured on the corresponding EBT3 film, whereas the focus position is determined from the measurements performed in air using the OTR screen. Simulations show that scattering in air has negligible effect on the position of the focal spot. The OTR diagnostic system was not used to estimate the beam size because it is not configured to store the full 2D beam profile, but only recorded the results of Gaussian fits in the horizontal and vertical plane, respectively. This data was not reliable because the electron beam profile was not Gaussian. The dose deposition is scored using a USBIN card<sup>56</sup> with resolution of 0.025 and 0.079 cm in the transverse and longitudinal directions, respectively. The dose is averaged within the volume of 0.025 × 30 cm<sup>2</sup> on the central beam axis. Simulations are performed for 10<sup>7</sup> histories and 5 cycles. The electron beam is mono-energetic and has a rectangular profile in the vertical plane for all *f*-numbers. The profile in the horizontal plane is Gaussian for *f*/12.3 and *f*/18.2 and rectangular for *f*/11.2. The PRECISION physics setting<sup>56</sup> is chosen to provide interaction models for all electromagnetic and nuclear processes that are relevant to the transport of VHEEs, including photonuclear interactions. The threshold for transport and production of delta particles and photons (ECUT, PCUT) is set to 10 keV with the EMCUT card<sup>56</sup>. Survival probability of a single photon produced via hadronic interactions is set to 0.002. The energy transfer to electrons lower than the threshold is estimated according to the continuous slowing down approximation<sup>57</sup>.

**Table 3 Optimised Twiss parameters and normalised emittance of the electron beams.**

	158 MeV		201 MeV	
	Horizontal	Vertical	Horizontal	Vertical
Beta (m)	9.03	5.88	11.40	5.30
Alpha	-1.73	0.25	-1.90	-0.18
Normalised emittance (π • mm • mrad)	6.80	6.90	5.80	11.40

**Table 4 Optimised gradients of the quadrupole magnets Q350-Q520.**

Quadrupole	Gradient (T/m)		
	158 MeV ( <i>f</i> /10.9)	158 MeV ( <i>f</i> /10.4)	201 MeV ( <i>f</i> /18.2)
Q350	8.55	8.55	0.00
Q355	10.26	10.26	11.40
Q360	0.00	0.00	0.00
Q510	11.40	11.40	2.31
Q515	8.04	8.21	7.17
Q520	10.49	11.06	10.98



**Fig. 5 Experimental setup.** Experimental setup (a) and EBT3 stack in the custom made holder (b). (1) focusing magnet, (2) vacuum window, (3) laser for beam alignment, (4) lead collimator, which was not used during irradiation, (5) ICT for charge measurement, (6) PMMA tank, (7) OTR screen, (8) motorised translation stage for transverse displacements of the PMMA tank, (9) CCD camera, (10) beam dump.

**Data availability**

Data associated with research published in this paper is available at <https://doi.org/10.15129/910256bd-3025-4c0d-bbba-faa08018db79>

Received: 9 November 2020; Accepted: 14 January 2021;

Published online: 23 February 2021

**References**

- Baskar, R., Dai, J., Wenlong, N., Yeo, R. & Yeoh, K.-W. Biological response of cancer cells to radiation treatment. *Front. Mol. Biosci.* **1**, 24 (2014).
- Otto, K. Volumetric modulated arc therapy: IMRT in a single gantry arc. *Med. Phys.* **35**, 310–317 (2008).
- Kondziolka, D. Current and novel practice of stereotactic radiosurgery. *J. Neurosurg.* **130**, 1789–1798 (2019).
- Pilar, A., Gupta, M., Laskar, S. G. & Laskar, S. Intraoperative radiotherapy: review of techniques and results. *Ecancermedscience* **11**, 750 (2017).
- Sethi, A. et al. Tissue inhomogeneity corrections in low-kV intra-operative radiotherapy (IORT). *Transl. Cancer Res.* **4**, 182–188 (2015).
- Skowronek, J. Current status of brachytherapy in cancer treatment - short overview. *J. Contemp. Brachyther.* **9**, 581–589 (2017).
- Muz, B., de la Puente, P., Azab, F. & Azab, A. K. The role of hypoxia in cancer progression, angiogenesis, metastasis, and resistance to therapy. *Hypoxia* **3**, 83–92 (2015).
- Schlegel, W., Grosser, K., Häring, P. & Rhein, B. Beam delivery in 3D conformal radiotherapy using multi-leaf collimators. In *New Technologies in Radiation Oncology* (eds. Schlegel, W. C., Bortfeld, T. & Grosu, A.-L.) 257–266 (Springer, 2006).
- Bragg, W. H. & Kleeman, R. On the alpha particles of radium and their loss of range in passing through various atoms and molecules. *Philos. Mag.* **10**, 600–602 (1905).
- Lomax, A. J. Charged particle therapy: the physics of interaction. *Cancer J.* **15**, 285–291 (2009).
- Bussiere, M. R. & Adams, J. A. Treatment planning for conformal proton radiation therapy. *Technol. Cancer Res. Treat.* **2**, 389–399 (2003).
- Kim, D.-H. et al. Proton range verification in inhomogeneous tissue: treatment planning system vs. measurement vs. Monte Carlo simulation. *PLoS ONE* **13**, e0193904 (2018).
- Zheng, Y. et al. Range uncertainty in proton therapy: an end-to-end study using various animal tissues. *Int. J. Radiat. Oncol. Biol. Phys.* **84**, S835 (2012).
- Papiez, L., DesRosiers, C. & Moskvina, V. Very high energy electrons (50–250 MeV) and radiation therapy. *Technol. Cancer Res. Treat.* **1**, 105–110 (2002).
- Bazalova-Carter, M. et al. Treatment planning for radiotherapy with very high-energy electron beams and comparison of VHEE and VMAT plans. *Med. Phys.* **42**, 2615–2625 (2015).
- Palma, B. et al. Evaluation of the performance of very high-energy electron (VHEE) beams in radiotherapy: five clinical cases. *Med. Phys.* **42**, 3568–3568 (2015).
- Palma, B. et al. Assessment of the quality of very high-energy electron radiotherapy planning. *Radiother. Oncol.* **119**, 154–158 (2016).
- Schüler, E. et al. Very high-energy electron (VHEE) beams in radiation therapy; Treatment plan comparison between VHEE, VMAT, and PPBS. *Med. Phys.* **44**, 2544–2555 (2017).
- Kokurewicz, K. et al. Focused very high-energy electron beams as a novel radiotherapy modality for producing high-dose volumetric elements. *Sci. Rep.* **9**, 10837 (2019).
- Hogstrom, K. R. & Almond, P. R. Review of electron beam therapy physics. *Phys. Med. Biol.* **51**, R455–R489 (2006).
- Diamantopoulos, S. et al. Clinical implementation of total skin electron beam (TSEB) therapy: a review of the relevant literature. *Phys. Med.* **27**, 62–68 (2011).
- Calvo, F. A. Intraoperative irradiation: precision medicine for quality cancer control promotion. *Radiat. Oncol.* **12**, 36–41 (2017).
- DesRosiers, C., Moskvina, V., Bielajew, A. F. & Papiez, L. 150–250 MeV electron beams in radiation therapy. *Phys. Med. Biol.* **45**, 1781–1805 (2000).
- Moskvina, V., Salvat, F., Stewart, D. K. & DesRosiers, C. M. PENELOPE Monte Carlo engine for treatment planning in radiation therapy with very high energy electrons (VHEE) of 150–250 MeV. *IEEE Nucl. Sci. Symp. Med. Imaging Conf.* 1961–1966, <https://doi.org/10.1109/NSSMIC.2010.5874117> (IEEE, 2010).
- Subiel, A. et al. Challenges of dosimetry of ultra-short pulsed very high energy electron beams. *Phys. Med.* **42**, 327–331 (2017).
- Subiel, A. et al. Dosimetry of very high energy electrons (VHEE) for radiotherapy applications: using radiochromic film measurements and Monte Carlo simulations. *Phys. Med. Biol.* **59**, 5811–5829 (2014).
- Kokurewicz, K. et al. Laser-plasma generated very high energy electrons (VHEEs) in radiotherapy. *Medical Applications of Laser-Generated Beams of Particles. IV: Review of Progress and Strategies for the Future* Vol. 10239 (ed. Ledingham, K. W. D.) UNSP 102390c <https://doi.org/10.1117/12.2271183> (SPIE, 2017).
- Lagzda, A. et al. Relative insensitivity to inhomogeneities on very high energy electron dose distributions. *Proceedings of IPAC 2017. THPVA139*. <https://doi.org/10.18429/JACoW-IPAC2017-THPVA139> (2017).
- Shiu, A. S. & Hogstrom, K. R. Dose in bone and tissue near bone-tissue interface from electron beam. *Int. J. Radiat. Oncol. Biol. Phys.* **21**, 695–702 (1991).
- Bova, F. J. Clinical electron beam physics. In *Radiation Therapy Physics* (ed. Smith, A. R.) 123–138 (Springer, 1995).
- Maxim, P. & Loo, B. Pluridirectional high-energy agile scanning electron radiotherapy (PHASER): extremely rapid treatment for early lung cancer. *DTIC Document* (2015).
- Faure, J. et al. A laser-plasma accelerator producing monoenergetic electron beams. *Nature* **431**, 541–544 (2004).
- Geddes, C. G. R. et al. High-quality electron beams from a laser wakefield accelerator using plasma-channel guiding. *Nature* **431**, 538–541 (2004).
- Mangles, S. P. D. et al. Monoenergetic beams of relativistic electrons from intense laser-plasma interactions. *Nature* **431**, 535–538 (2004).
- Labate, L. et al. Toward an effective use of laser-driven very high energy electrons for radiotherapy: feasibility assessment of multi-field and intensity modulation irradiation schemes. *Sci. Rep.* **10**, 17307 (2020).
- Jaroszynski, D. A. et al. Radiation sources based on laser-plasma interactions. *Philos. Trans. R. Soc. A* **364**, 689–710 (2006).
- Bostick, W. Possible techniques in direct-electron-beam tumor therapy. *Phys. Rev.* **77**, 564 (1950).
- Weinhaus, M. S., Nath, R. & Schulz, R. J. Enhancement of electron-beam dose distributions by longitudinal magnetic-fields - Monte-Carlo simulations and magnet system optimization. *Med. Phys.* **12**, 598–603 (1985).
- Shih, C. High energy electron radiotherapy in a magnetic field. *Med. Phys.* **2**, 9–13 (1975).
- Gamba, D. et al. The CLEAR user facility at CERN. *Nucl. Instrum. Methods Phys. Res. A* **909**, 480–483 (2018).
- Symonds, P. & Jones, G. FLASH radiotherapy: the next technological advance in radiation therapy? *Clin. Oncol.* **31**, 405–406 (2019).
- Brunetti, E. et al. A simple method of producing a focused x-ray beam. Vol. 11036, SPIE Optics & Optoelectronics, (SPIE, 2019).
- Tajima, T. & Dawson, J. M. Laser electron accelerator. *Phys. Rev. Lett.* **43**, 267 (1979).
- Brunetti, E. et al. Low emittance, high brilliance relativistic electron beams from a laser-plasma accelerator. *Phys. Rev. Lett.* **105**, 215007 (2010).
- Li, Y. et al. Generation of 20 kA electron beam from a laser wakefield accelerator. *Phys. Plasmas* **24**, 023108 (2017).
- Leemans, W. et al. Multi-GeV electron beams from capillary-discharge-guided subpetawatt laser pulses in the self-trapping regime. *Phys. Rev. Lett.* **113**, 245002 (2014).
- Islam, M. et al. Near-threshold electron injection in the laser-plasma wakefield accelerator leading to femtosecond bunches. *N. J. Phys.* **17**, 093033 (2015).
- Wiggins, S. et al. Note: Femtosecond laser micromachining of straight and linearly tapered capillary discharge waveguides. *Rev. Sci. Instrum.* **82**, 096104 (2011).
- Gonsalves, A. et al. Petawatt laser guiding and electron beam acceleration to 8 GeV in a laser-heated capillary discharge waveguide. *Phys. Rev. Lett.* **122**, 084801 (2019).
- Welsh, C., Bravin, E. & Lefevre, T. Investigations of OTR screen surfaces and shapes. *10th European Particle Accelerator Proceedings, EPAC Conf. Proc. C 060626 1220–1222* (CERN, 2006).
- Qin, H. & Davidson, R. C. Generalized Courant-Snyder theory for coupled transverse dynamics of charged particles in electromagnetic focusing lattices. *Phys. Rev. ST Accel. Beams* **12**, 064001 (2009).
- Qin, H. & Davidson, R. C. A physical parametrization of coupled transverse dynamics based on generalized Courant-Snyder theory and its applications. *Phys. Plasmas* **16**, 050705 (2009).
- Skelton, S. Multi-quadrupole scan for emittance determination at PITZ. *DESY Summer Student Report* (University of St Andrews, 2007).
- Deniau, L. & Grote, H. The MAD-X Program. *User's Reference Manual*. (ELPH, 2017).
- Schuller, A., Makowski, C., Kapsch, R. P., Nolte, R. & Beck, P. MELAF—a 50 MeV electron accelerator facility for research in radiation effects. *17th European Conf. Radiation and its Effects on Components and Systems (RADECS)*, 239–242 (IEEE, 2017).
- Battistoni, G. et al. Overview of the FLUKA code. *Ann. Nucl. Energy* **82**, 10–18 (2015).
- Berger, M. J. et al. Report 37: stopping powers for electrons and positrons. *J. Int. Commission on Radiation Units and Measurements os19*, <https://doi.org/10.1093/jicru/os19.2.Report37> (1984).

## Acknowledgements

We acknowledge support of the U.K. EPSRC (grant nos. EP/J018171/1, EP/J500094/1 and EP/N028694/1) and the EC's LASERLAB-EUROPE (grant nos. 654148 and 871124).

## Author contributions

D.A.J. conceived the investigation; K.K. and E.B. carried out simulations; K.K., E.B., A.C., D.G., L.G., A.G., E.S., K.N.S., W.F. and R.C. carried out experiments; K.K. and E.B. designed the experimental equipment and W.F. designed and prepared the CERN test beamline. K.K. and E.B. performed the data analysis; K.K., E.B. and D.A.J. interpreted the results; K.K., E.B. and D.A.J. wrote the manuscript, with all other authors contributing; D.A.J. provided overall supervision.

## Competing interests

The authors declare no competing interests.

## Additional information

**Supplementary information** The online version contains supplementary material available at <https://doi.org/10.1038/s42005-021-00536-0>.

**Correspondence** and requests for materials should be addressed to E.B. or D.A.J.

**Reprints and permission information** is available at <http://www.nature.com/reprints>

**Publisher's note** Springer Nature remains neutral with regard to jurisdictional claims in published maps and institutional affiliations.



**Open Access** This article is licensed under a Creative Commons Attribution 4.0 International License, which permits use, sharing, adaptation, distribution and reproduction in any medium or format, as long as you give appropriate credit to the original author(s) and the source, provide a link to the Creative Commons license, and indicate if changes were made. The images or other third party material in this article are included in the article's Creative Commons license, unless indicated otherwise in a credit line to the material. If material is not included in the article's Creative Commons license and your intended use is not permitted by statutory regulation or exceeds the permitted use, you will need to obtain permission directly from the copyright holder. To view a copy of this license, visit <http://creativecommons.org/licenses/by/4.0/>.

© The Author(s) 2021